Journal of Power Sources 209 (2012) 72–80

Contents lists available at SciVerse ScienceDirect

Journal of Power Sources

journal homepage: www.elsevier.com/locate/jpowsour

Durable copper–zinc catalysts modified with indium oxide in high temperature steam reforming of methanol for hydrogen production

Yasuyuki Matsumura [a,*], Hideomi Ishibe [b]

[a] National Institute of Advanced Industrial Science and Technology (AIST), Kansai Center, Midorigaoka, Ikeda, Osaka 563-8577, Japan
[b] Nippon Seisen Co., Ltd., Hirakata Plant, Ikenomiya, Hirakata, Osaka 573-8522, Japan

ARTICLE INFO

Article history:
Received 20 December 2011
Received in revised form 16 February 2012
Accepted 20 February 2012
Available online 1 March 2012

Keywords:
Methanol steam reforming
$Cu/ZnO/ZrO_2$
Indium oxide
Stabilization
Hydrogen production

ABSTRACT

The catalytic activity of Cu/ZnO decreases gradually in the high temperature steam reforming of methanol to hydrogen and carbon dioxide at 400 °C or above. Addition of indium oxide to Cu/ZnO results in significant deactivation of the Cu surface. The turnover frequency (TOF) of the catalyst containing 4 wt.% of In_2O_3 is reduced to ca. 1/10, but the activity is stabilized. Partial aggregation of indium oxide takes place during the reaction. Presence of zirconium oxide in the catalytic system greatly mitigates the deactivation with indium oxide. The activity of $Cu/ZnO/ZrO_2$ is also stabilized by the addition of indium oxide, and the by-production of carbon monoxide is significantly suppressed. No aggregation of indium oxide particles occurs in the presence of zirconium oxide. The activity of $Cu/ZnO/ZrO_2$ modified with 2 wt.% of indium oxide is comparable to that of the unmodified Cu/ZnO.

1. Introduction

Hydrogen is an important chemical mainly used in industries for synthesis of methanol and ammonia, desulfurization of petroleum, hydrogenation of chemicals, reduction processes in metallurgy, etc. On the other hand, hydrogen has been considered as a future energy resource especially for fuel cells to produce electricity [1]. Polymer electrolyte fuel cells (PEFCs) have been developed mainly due to their portability and application for automobiles. However, storage of hydrogen in keeping compactness is difficult technology; for example, on-board hydrogen storage vessels require working pressure higher than 35 MPa and the development of the vessels is still challenging [2]. The alternative solution is on-board hydrogen processing from liquid energy carriers such as methanol, dimethyl ether, and gasoline [3]. Steam reforming of methanol to hydrogen ($CH_3OH + H_2O \rightarrow 3\,H_2 + CO_2$) is advantageous for the hydrogen production because the reaction is usually selective over copper catalysts such as $Cu/ZnO/Al_2O_3$ [4]. In general, the reaction is carried out at a temperature lower than 300 °C and thermal oil is employed for the heat supply to a conventional reformer to prevent overheating which causes the deactivation of the copper catalysts [4,5]. It is advantageous for a compact reformer to be directly heated with combustion gas because of the simplicity and the thermal efficiency [6]. However, the reactor temperature is hard to be controlled and often exceeds 300 °C. In addition, the reactor in the on-board processor needs to be immediately heated up to the reaction temperature under daily start and stop (DSS) operation mode. Yang et al. reported that $ZnO—Al_2O_3$ is active to the methanol steam reforming around 400 °C, but the activity is steeply decreases with a decrease in the reaction temperature probably because of the high activation energy [7].

We studied the activity of Cu/ZnO and $Cu/ZnO/ZrO_2$ in the high temperature reforming mainly at 400 °C and found that the reduction of the activity in the initial stage of the reaction is mainly due to the decrease in the surface activity of copper [8,9]. Hence, the stabilization of the surface activity is important for the stable activity at 400 °C as well as prevention of the sintering which causes a decrease in the Cu surface area.

Indium oxide is known to be active to the steam reforming of methanol and ethanol; low selectivity to carbon monoxide, which is unfavorable byproduct against PEFCs, was reported in the methanol reforming even at 400 °C [10,11]. Addition of indium to palladium produces the selective and stable activity to methanol steam reforming [12]. Nevertheless, the effect of indium to copper has not been investigated. In the present work, we added indium oxide to Cu/ZnO and $Cu/ZnO/ZrO_2$ and examined the activity at 400 °C. It is shown that addition of indium oxide to $Cu/ZnO/ZrO_2$ significantly stabilizes the catalytic activity and suppresses the by-production of carbon monoxide.

* Corresponding author. Tel.: +81 72 751 7821; fax: +81 72 751 9623.
E-mail address: yasu-matsumura@aist.go.jp (Y. Matsumura).

0378-7753/$ – see front matter © 2012 Elsevier B.V. All rights reserved.
doi:10.1016/j.jpowsour.2012.02.084

2. Experimental

A Cu/ZnO catalyst (CZ) was prepared by coprecipitation from a 0.5-M aqueous mixture of $Cu(NO_3)_2{\cdot}3H_2O$ (Wako Pure Chemical, S grade) and $Zn(NO_3)_2{\cdot}6H_2O$ (Wako, S) with addition of an aqueous solution of Na_2CO_3 (0.5 M) under vigorous stirring at 80 °C as described elsewhere [9]. After filtration and washing with distilled water, the precipitate was dried at 120 °C for 15 h and finally calcined in air at 500 °C for 12 h. The Cu content was 50 wt.% in the reduced form. Indium oxide was introduced to Cu/ZnO by addition of $In(NO_3)_3{\cdot}9H_2O$ (Wako, 98 + %) to the starting solution of CZ. The contents of In_2O_3 and Cu in the catalyst (4In-CZ) were 4 and 48 wt.%, respectively, in the reduced catalyst. Zirconium and indium oxides were added to Cu/ZnO by the coprecipitation from the starting solution also containing $ZrO(NO_3)_2{\cdot}2H_2O$ (Wako, 1st). Two $Cu/ZnO/ZrO_2$ catalysts containing 2 and 5 wt.% In_2O_3 (2In-CZZ and 5In-CZZ, respectively) were prepared and both the contents of Cu and ZnO in the reduced catalysts were fixed at 30 wt.%.

Catalytic tests were performed in a fixed-bed continuous-flow reactor operated under atmospheric pressure as described elsewhere [8,9]. Zirconia balls (1 mm in diameter) were mixed with a powder catalyst (50–100 mesh) whose weight (W) was 0.20–0.50 g to reduce back pressure during the reaction and keep sufficient length of the catalyst layer (2.0 g in total of the catalyst and the balls). The catalyst was usually pre-reduced with a reaction mixture of methanol, steam, and argon (1.0/1.2/0.5 in molar ratio) with a flow rate (F) of 27 $dm^3\ h^{-1}$ at 250 °C for 1 h; then the reactor was heated up to 400 °C in the reaction flow. The effluent gas was dried with a cold trap at ca. −50 °C, and analyzed with an on-stream gas chromatograph. After the reaction for 7 h, the catalyst was cooled to room temperature under an Ar stream. When the catalyst was pre-reduced with hydrogen, a stream of 10-vol.% hydrogen diluted with argon (6.0 $dm^3\ h^{-1}$) was fed at 400 °C for 1 h.

The methanol conversion (C) was determined from the material balance of the reactant and the products. The error was within 5%. No formation of formaldehyde or methyl formate was observed. The selectivities of CO and CH_4 (S_{CO} and S_{CH_4}, respectively) were calculated from the equations, $S_{CO} = Y_{CO}/Y_{CO_2} + Y_{CO} + Y_{CH_4}$ and $S_{CH_4} = Y_{CH_4}/Y_{CO_2} + Y_{CO} + Y_{CH_4}$ where Y_{CO_2}, Y_{CO}, and Y_{CH_4} are yields of CO_2, CO, and CH_4, respectively, in molar basis. The hydrogen yield (Y) was calculated from the equation, $Y = C(1 - 1/3S_{CO} - 4/3S_{CH4})$.

Powder X-ray diffraction (XRD) patterns of the Cu catalysts were recorded in air at room temperature with an MAC Science MP6XCE diffractometer using nickel-filtered Cu Kα radiation.

X–ray photoelectron spectra (XPS) of the Cu catalysts were recorded at room temperature with a JEOL JPS-9010MX spectrometer (Al Kα). After the reaction, the catalyst sample was taken out from the reactor and mounted in air to a sample holder. Since the sample was gradually oxidized in air, Ar sputtering (400 V, 7 mA) was performed for 5 s to remove oxygen adsorbed on the surface. The sample reduced with hydrogen at 400 °C for 1 h was mounted to a sample holder under Ar atmosphere and measured without the Ar sputtering. Binding energy was corrected by the reference of the C 1s line at 284.6 eV. The surface atomic concentrations of Cu, Zn, Zr, In, and O were calculated from the peak areas using the average matrix relative sensitivity factors (AMRSFs) of Cu $2p_{3/2}$ (32), Zn $2p_{3/2}$ (39), Zr 3d (5.5), In $3d_{5/2}$ (39), and O 1 s (3.4). Since the peak intensity relates to the electron inelastic mean free path of electron for the surface substance, the surface concentrations were corrected using the values of 2.1 nm (Cu), 2.7 nm (ZnO and ZrO_2), and 2.3 nm (In_2O_3) [13]. The AMRSFs were determined by measuring standard materials of Cu, Zn, Zr, and In metal plates and an alumina plate. The uncertainty of AMRSFs is less than 2% [13].

The BET surface areas of the Cu catalysts were determined from the N_2 physisorption isothermes.

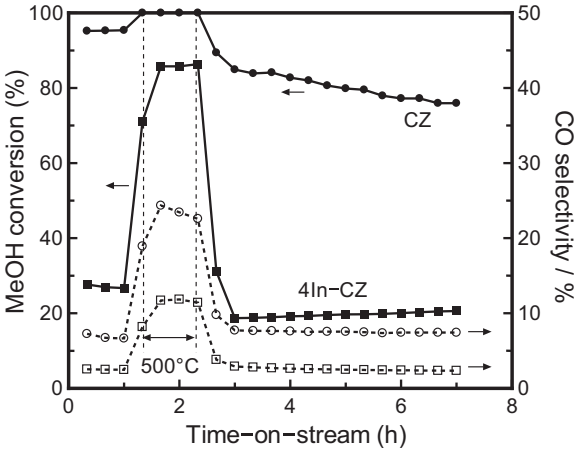

Fig. 1. Catalytic activities of Cu/ZnO modified and unmodified with indium oxide in methanol steam reforming mainly at 400 °C. F/W, 55 $dm^3\ h^{-1}\ g^{-1}$. Circle symbols, CZ; square, 4In-CZ.

The structures of the Cu catalysts after the reaction were evaluated by transmission electron microscopy (TEM) and high-angle annular dark field imaging in scanning TEM (HAADF/STEM) with energy dispersed X-ray spectroscopic (EDS) analysis using an FEI Tecnai G^2 F20 Twin with an EDX detecting unit (EDAX Inc.) at the acceleration voltage of 200 kV.

The profiles of extended X-ray absorption fine structure (EXAFS) for the catalysts containing indium oxide were taken at room temperature in the transmission mode for In K-edge at beam-line BL14B2 of SPring-8 with the approval of the Japan Synchrotron Radiation Research Institute (JASRI) (Proposal No. 2009B1962). The sample was handled in air and vacuum-sealed with polyethylene films. The Fourier transformation was performed on k^3-weighted EXAFS oscillations in the range of 30–120 nm^{-1}. Normalization of the EXAFS function was done by dividing the absorption intensity by the height of the absorption edge. A cubic spline background subtraction was carried out. The data analysis was performed with a program of "REX2000" supplied by Rigaku.

3. Results

3.1. Steam reforming of methanol over the Cu catalysts

Steam reforming of methanol to hydrogen and carbon dioxide was carried out over Cu/ZnO (CZ) at 400 °C for 1 h and the reaction temperature was risen to 500 °C to enhance the deactivation; then, the activity at 400 °C was tested (Fig. 1). The methanol conversion decreases to 76% after 7 h-on-stream (F/W, 55 $dm^3\ h^{-1}\ g^{-1}$). Carbon monoxide is by-produced and the selectivity is 7.4% at the end of the reaction. The hydrogen yield is 74%. Slight formation of methane with the selectivity of 0.04–0.06% is detected in the reaction at 500 °C and it is 0.02% at 400 °C after the reaction at 500 °C. The addition of In_2O_3 drastically decreases the activity of Cu/ZnO, but the methanol conversion with 4In-CZ is discernibly increased from 18.7% at 3 h-on-stream to 20.5% at 7 h-on-stream. The CO selectivity is decreased from 2.9% to 2.3%. The selectivity to methane is 1.1% at 500 °C and it is 0.2% at 400 °C after the deactivation at 500 °C.

Presence of zirconium oxide in the catalytic system greatly mitigates the deactivation by the In_2O_3 addition with the stable activity (Fig. 2). In the case of 2In-CZZ, the final conversion is 79% being higher than that of CZ and the CO selectivity is as small as 1.7% with the CH_4 selectivity of 0.02%. The hydrogen yield is 78% and almost the same as the methanol conversion. The methane selectivity at 500 °C is 0.1%. The higher content of In_2O_3 results in the lower activity; that is, 5In-CZZ produces the methanol conversion

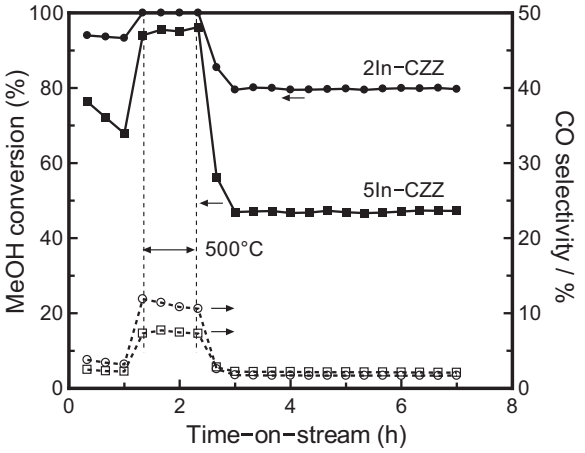

Fig. 2. Catalytic activities of In_2O_3-modified $Cu/ZnO/ZrO_2$ in methanol steam reforming mainly at 400 °C. F/W, 55 $dm^3\ h^{-1}\ g^{-1}$. Circle symbols, 2In-CZZ; square, 5In-CZZ.

of 47% at the end of the reaction with the CO selectivity of 2.1%. The methane selectivity is 0.09% and it is 0.2% at 500 °C.

The reactions with 2In- and 5In-CZZ were carried out under different contact times (Fig. 3). The CO selectivities for 2In-CZZ and 5In-CZZ are around 2%.

The activity of 5In-CZZ reduced with hydrogen at 400 °C for 1 h was separately tested at 400 °C for 7 h. The initial conversion is 44% with the CO selectivity of 2.5% at the F/W of 78 $dm^3\ h^{-1}\ g^{-1}$ and the conversion decreases gradually to 42% with the CO selectivity of 2.1% at the end of the reaction. The methane selectivity is always 0.1%.

3.2. XRD of the Cu catalysts

Peaks for metallic Cu are recorded at 43.4° and 50.6° in 2θ with the peaks attributed to ZnO in the XRD pattern of CZ after the reaction for 7 h (Fig. 4) [14]. The patterns for 4In-CZ are similar to that for CZ, but a small peak at 30.6° appears for the sample after 7 h-on-stream.

Peaks for metallic Cu and ZnO are also present in the patterns for 2In- and 5In-CZZ (Figs. 5 and 6). A weak and broad peak attributed to tetragonal ZrO_2 is present at 30–31° for 2In-CZZ just after the reduction with the reaction feed at 250 °C for 1 h [14]. The peak is significantly intensified after 7 h-on-stream. The same phenomenon can be observed with 5In-CZZ. The mean crystallite

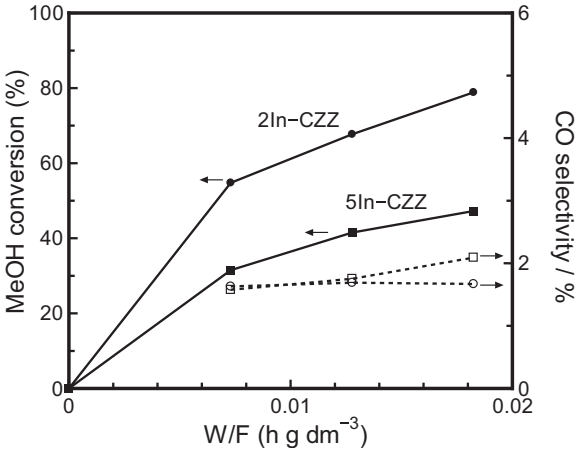

Fig. 3. Dependence of the catalytic activity of In_2O_3-modified $Cu/ZnO/ZrO_2$ on contact time (W/F). Time-on-stream, 7 h. Circle symbols, 2In-CZZ; square, 5In-CZZ.

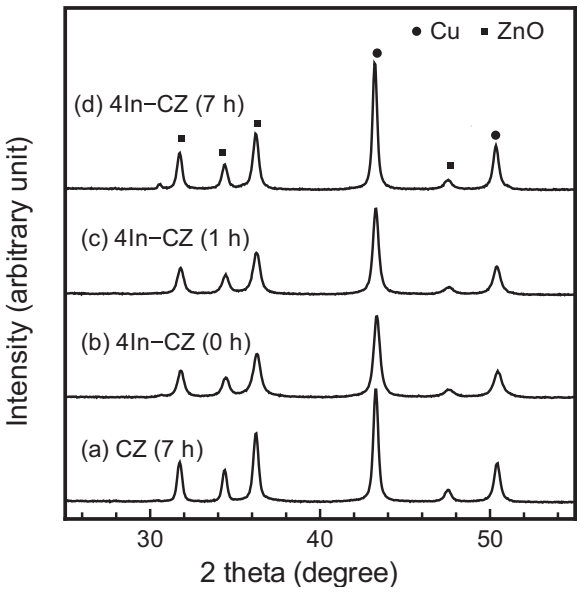

Fig. 4. XRD patterns of Cu/ZnO modified and unmodified with indium oxide. (a) CZ after reaction for 7 h, (b) 4In-CZ after reduction with the reaction feed at 250 °C for 1 h, (c) after reaction for 1 h, and (d) after reaction for 7 h.

sizes of Cu, ZnO, and ZrO_2 are calculated from the line broadening at 43.4°, 36.4°, and 30–31°, respectively, using Scherrer equation (Table 1) [15]. The size of Cu for 4In-CZ after the reaction for 7 h is similar to that of CZ, but it is significantly larger than those for 2In- and 5In-CZZ. The size of ZnO for 4In-CZ is also larger than those for In-CZZ.

3.3. Surface analyses of the Cu catalysts

The surface of the 5In-CZZ was characterized by XPS. The binding energy of Cu $2p_{3/2}$ is 932.5 eV for the sample reduced with hydrogen at 400 °C for 1 h. Since the binding energy is close to those for Cu metal (932.67 eV) and Cu_2O (932.4 eV) [16], the Auger line of Cu L_3VV is recorded to identify the oxidation state. The kinetic energy is 918.6 eV, whereas the energies for Cu metal and Cu_2O are

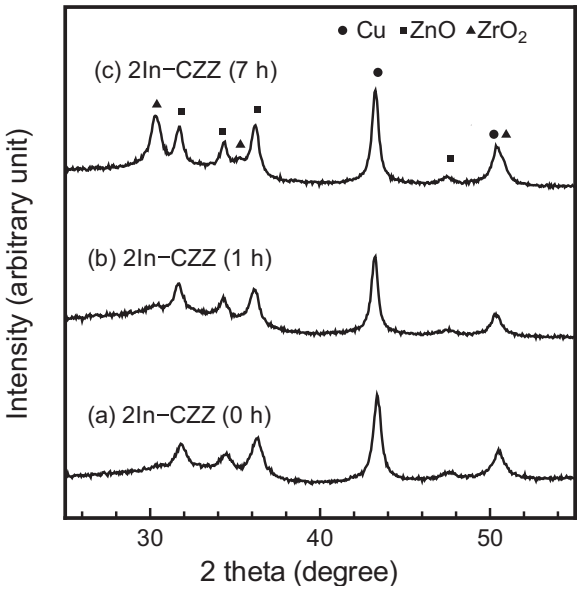

Fig. 5. XRD patterns of 2In-CZZ. (a) After reduction with the reaction feed at 250 °C for 1 h, (b) after reaction for 1 h, and (c) after reaction for 7 h.

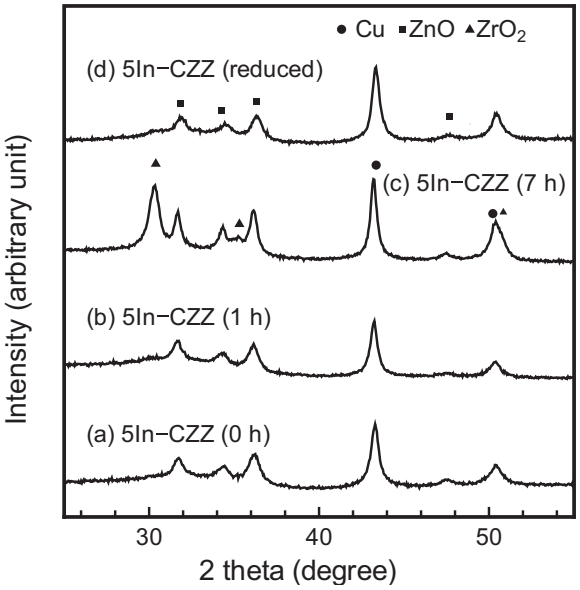

Fig. 6. XRD patterns of 5In-CZZ. (a) After reduction with the reaction feed at 250 °C for 1 h, (b) after reaction for 1 h, (c) after reaction for 7 h, and (d) after reduction with hydrogen at 400 °C for 1 h.

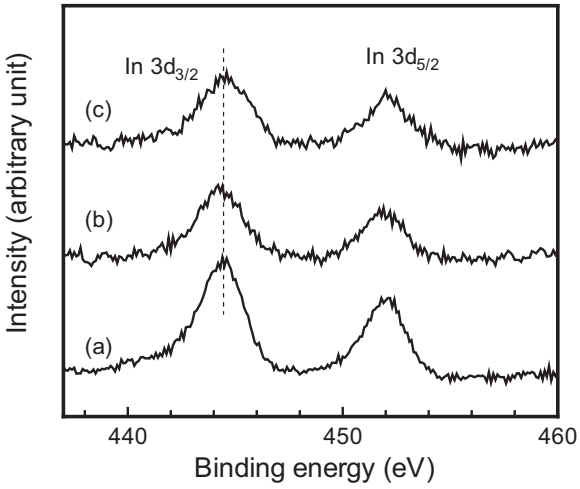

Fig. 7. XPS of In 3d region for 5In-CZZ. (a) As prepared, (b) after reduction with hydrogen at 400 °C for 1 h, and (c) after contact with air following the hydrogen reduction.

918.65 and 916.8 eV, respectively [16]. The α value (Auger parameter + photon energy) is 1851.1 eV, showing that the surface species is metallic; the values for metallic Cu andCu_2O are 1851.3 and 1849.4 eV, respectively [16]. The binding energies of Zn $2p_{3/2}$ and Zr $2p_{3/2}$ are 1021.8 and 182.4 eV, respectively. The binding energy of In $3d_{5/2}$ for unreduced 5In-CZZ is 444.5 eV with 1021.9 eV for Zn $2p_{3/2}$ (Fig. 7a) and that for the reduced sample is 444.2 eV (Fig. 7b). The α value (Cu) became 1850.5 eV after short contact with air at room temperature, suggesting that the surface reduced with hydrogen is partly oxidized with air; the energy for Zn $2p_{3/2}$ is 1021.8 eV. The binding energy of In $3d_{5/2}$ for this sample is 444.4 eV (Fig. 7c).

The surface atomic concentrations determined by XPS are summarized in Table 2. As shown in the XRD patterns of the Cu catalysts after the reaction (see Figs. 4–6), the bulk of the Cu particles are metallic even in air while the surface is gradually oxidized. After the Ar sputtering, the α values (Cu) for the samples are always 1850.9–1851.3 eV, showing that the surface of Cu particles becomes metallic [9]. The concentration of Cu is 19% for CZ after the reaction for 7 h and similar to that for 4In-CZ. The Cu concentrations for 2In- and 5In-CZZ are 7–9%. The surface concentration of In^{3+} for 4In-CZ is 1–2%, and those for 2In- and 5In-CZZ are 0.2–0.3% and 0.5–0.6%, respectively.

The BET surface area of 4In-CZ is decreased from 20 to 9 $m^2\ g^{-1}$ during the reaction for 7 h (Table 3). The surface areas for 2In-CZZ are significantly higher than those for 4In-CZ and close to those for 5In-CZZ.

3.4. TEM and HAADF/STEM analyses of In_2O_3-modified Cu catalysts

The TEM and HAADF/STEM images of 4In-CZ after the reaction for 7 h shows that particles are considerably aggregated (Fig. 8) and the small particles at points 1 and 2 mainly contain Cu and the particle at point 3 mainly contains Zn. A grain (point 4) mainly contains Cu and Zn, suggesting presence of Cu and ZnO particles in the grain. Indium is slightly detected in these points. While the structure in Fig. 8 was mainly observed with the sample, we found a large lump containing indium significantly (Fig. 9, points 1 and 2). The In content is small in a grain (point 3) near the lump and it is slight at the point 4.

Fine particles with the size of 5–10 nm are seen in the TEM image of 2In-CZZ after the reaction for 7 h (Fig. 10). In a part of the fine particles (point 1), Zr is detected with Cu and Zn. There are mainly Cu and Zn at the points 2–4. Indium is slightly detected at the points 1 and 2, while no significant particles or grains obviously containing In were found.

Table 1
Mean crystallite sizes of the catalysts after reaction mainly at 400 °C. The sizes were determined from the XRD peaks of Cu(1 1 1), Zn(1 0 0), and ZrO_2(1 1 1).

Catalyst	Time-on-stream/h	Mean crystallite size/nm		
		Cu	ZnO	ZrO_2
CZ	7	26	24	–
4In-CZ	0[a]	19	20	–
4In-CZ	1	21	20	–
4In-CZ	7	28	22	–
2In-CZZ	0[a]	16	11	5
2In-CZZ	1	18	13	5
2In-CZZ	7	18	14	10
5In-CZZ	0[a]	16	12	–
5In-CZZ	1	18	13	5
5In-CZZ	7	19	17	12
5In-CZZ	Reduced[b]	15	12	–

[a] After reduction with the reaction feed at 250 °C for 1 h.
[b] After reduction with hydrogen at 400 °C for 1 h.

Table 2
Surface atomic concentrations of the catalysts after reaction at 400 °C.

Catalyst	Time-on-stream/h	Surface atomic concentration (%)			
		Cu	Zn^{2+}	Zr^{4+}	In^{3+}
CZ	7	19	20	–	–
4In-CZ	0[a]	16	26	–	1.5
4In-CZ	1	16	19	–	1.3
4In-CZ	7	20	17	–	1.9
2In-CZZ	0[a]	8.6	14	15	0.2
2In-CZZ	1	8.4	14	17	0.2
2In-CZZ	7	7.4	12	20	0.3
5In-CZZ	0[a]	6.8	12	14	0.5
5In-CZZ	1	8.3	16	16	0.5
5In-CZZ	7	8.6	13	19	0.6
5In-CZZ	Reduced[b]	7.6	16	17	0.6

[a] After reduction with the reaction feed at 250 °C for 1 h.
[b] After reduction with hydrogen at 400 °C for 1 h.

Table 3
BET surface areas and reaction parameters of the catalysts after reaction at 400 °C.

Catalyst	Time-on-stream (h)	BET surface area ($m^2\ g^{-1}$)	Cu surface amount[a] ($mmol\ g^{-1}$)	MeOH consumption rate[b] ($mmol\ s^{-1}\ g^{-1}$)	TOF[c] (s^{-1})
CZ	7	12	0.08	0.40	5
4In-CZ	0[d]	20	0.1_2	0.047	0.4
4In-CZ	1	19	0.1_0	0.045	0.5
4In-CZ	7	9	0.06	0.032	0.5
2In-CZZ	0[d]	52	0.1_6	1.2	7
2In-CZZ	1	49	0.1_5	0.89	6
2In-CZZ	7	37	0.1_0	0.43	4
5In-CZZ	0[d]	53	0.1_3	0.40	3
5In-CZZ	1	48	0.1_5	0.26	2
5In-CZZ	7	37	0.1_2	0.12	1
5In-CZZ	Reduced[e]	57	0.1_6	0.14	0.8

[a] The amount was determined from the surface atomic concentration and BET surface area.
[b] Methanol consumption rate at the methanol conversion of 50%.
[c] TOF at the methanol conversion of 50%.
[d] After reduction with the reaction feed at 250 °C for 1 h.
[e] After reduction with hydrogen at 400 °C for 1 h.

3.5. Structural analyses of indium in In_2O_3-modified Cu catalysts by EXAFS

In order to analyze the atomic structure of indium in the Cu catalysts, EXAFS analysis was performed. The peak attributed to In—O interaction is present at 0.17 nm (peak shift uncorrected) in the Fourier transform of 4In-CZ just after the reduction with the reaction feed at 250 °C for 1 h (Fig. 11a). A shoulder at ca. 0.2 nm is appeared with the sample after the reaction at 400 °C for 1 h (Fig. 11b), and the shoulder is intensified in the sample after the

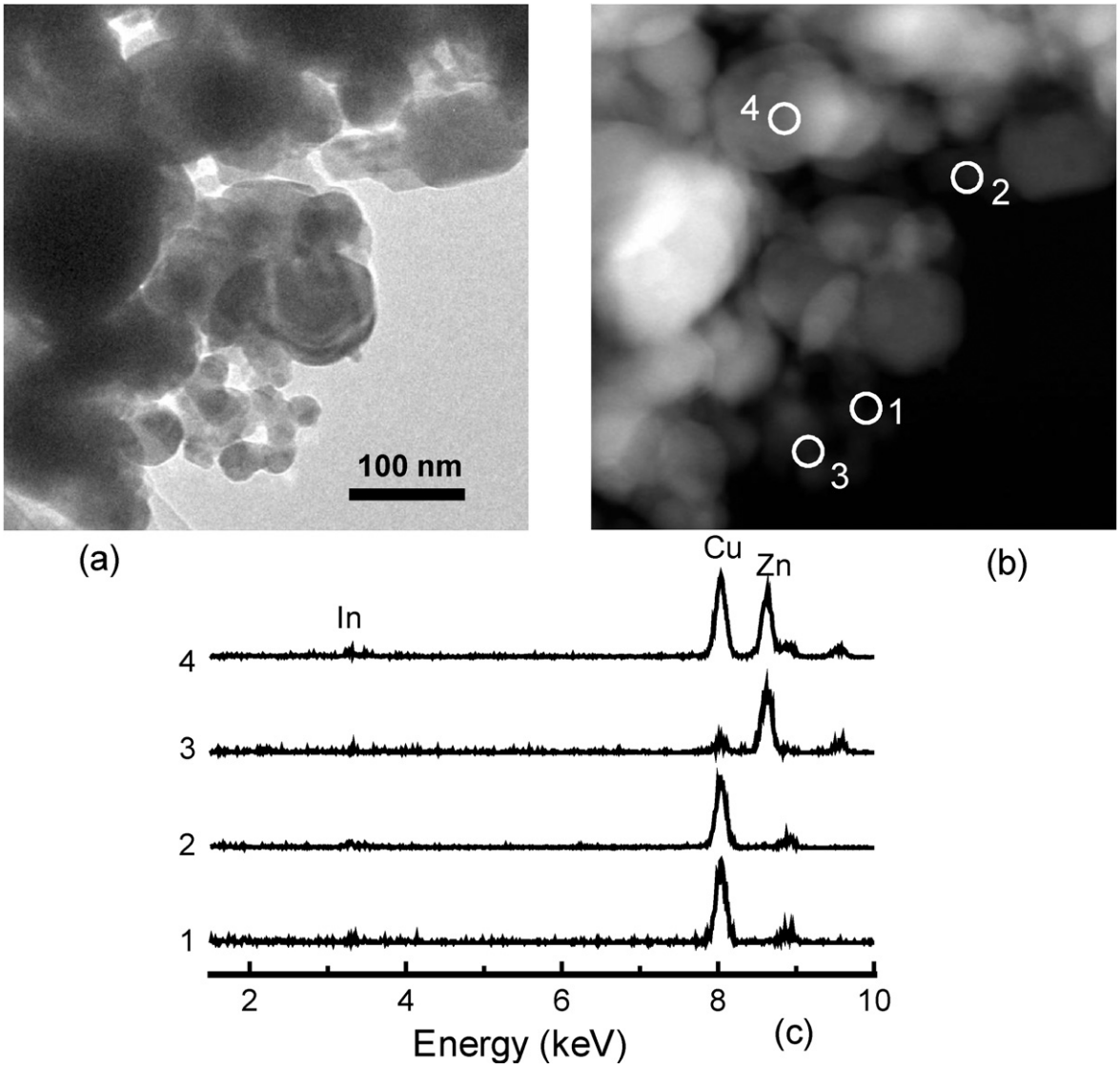

Fig. 8. TEM and HAADF/STEM images and EDS analysis of 4In-CZ after reaction for 7 h. (a) TEM image, (b) HAADF/STEM image, and (c) EDS spectra on points 1–4.

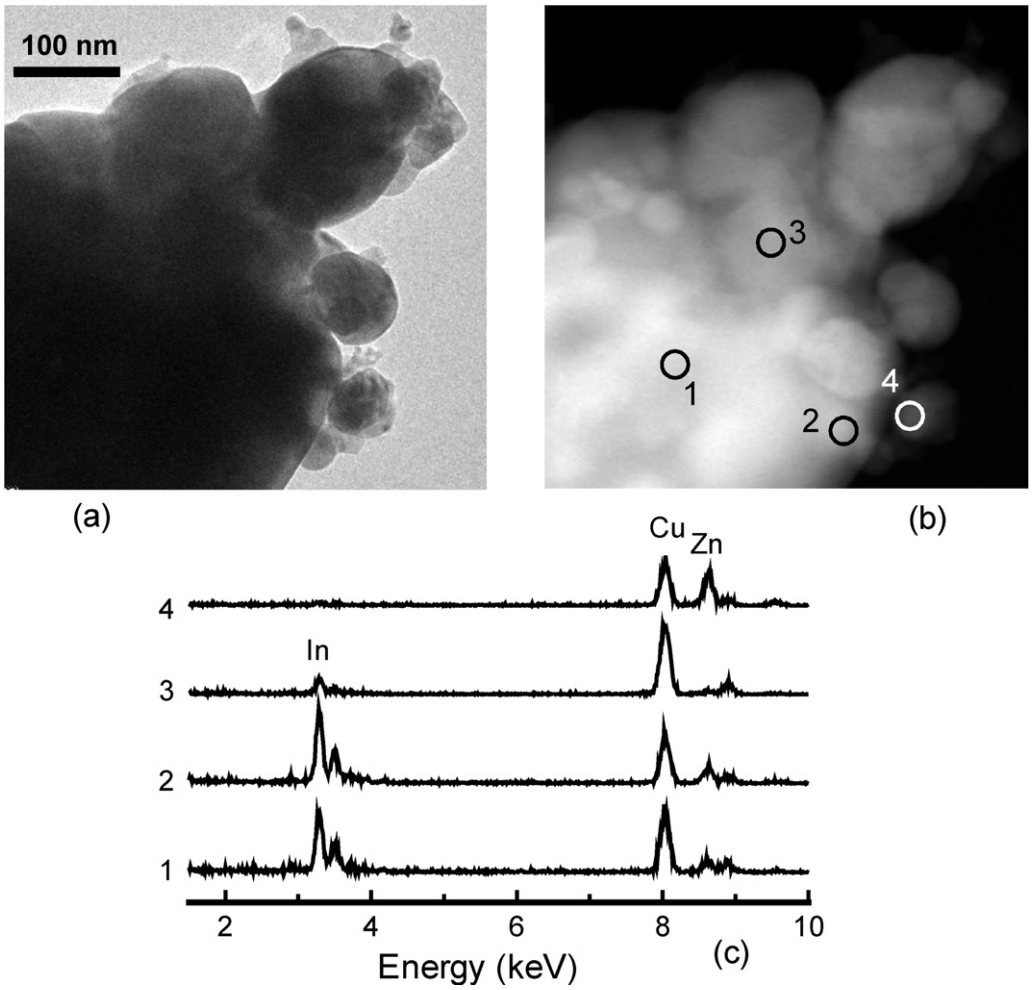

Fig. 9. TEM and HAADF/STEM images and EDS analysis of a different portion of 4In-CZ shown in Fig. 8. (a) TEM image, (b) HAADF/STEM image, and (c) EDS spectra on points 1–4.

reaction for 7 h (Fig. 11c). The In—In interaction is present at 0.31 nm in the Fourier transform of the In_2O_3 standard (Fig. 11d), but the interaction is weak in the profiles for 4In-CZ.

In the case of 2In-CZZ after the reaction for 7 h, no shoulder at 0.2 nm appears, but the magnitude of the peak at 0.17 nm is significantly smaller than that for the sample after the reaction for 1 h (Fig. 12). The magnitude for 5In-CZZ is discernibly decreased after the reaction for 7 h, while a considerable decrease is observed with the sample just after the reduction with hydrogen at 400 °C for 1 h (Fig. 13).

4. Discussion

4.1. Surface amount of copper on the catalyst

The Cu surface amount is usually determined by the N_2O decomposition on the basis of the stoichiometry, $N_2O + 2\,Cu \rightarrow N_2 + 2\,Cu_2O$ [17]. However, it is suggested that N_2O is also consumed for the oxidation of indium oxide partially reduced with hydrogen, because the binding energy of In $3d_{5/2}$ for 5In-CZZ just after the reduction is 444.2 eV and the energy increases to 444.4 eV after contact with air; the binding energy for metallic In is 443.8 eV [16]. The small peak at 0.17 nm in the Fourier transform of 5In-CZZ after the H_2 reduction (see Fig. 13d) indicates decrease in the In—O interaction due to the partial reduction.

The Cu surface amount can be estimated from the surface atomic concentrations and the BET surface area [8,9]. The Cu surface amount is calculated using the atomic site densities that are assumed as 0.032 mmol m^{-2} (Cu), 0.097 mmol m^{-2} (Zn^{2+}), 0.085 mmol m^{-2} (Zr^{4+}), 0.081 mmol m^{-2} (In^{3+}), and 0.030 mmol m^{-2} (O^{2-}) on the basis of the atomic/ionic radii. While the surface atomic concentrations do not reflect the bulk structure, it is considered that the particle distribution is rather homogeneous in coprecipitated catalysts and the surface atomic concentrations for the inner surface are similar to those for the outer surface. In actual, we determined the Cu surface amounts for coprecipitated Cu/ZnO and Cu/ZnO/ZrO_2 with this technique in other experiment [9], and the values corresponded with those determination by N_2O decomposition fairly well. Hence, it is at least available for comparison purpose.

4.2. Normalization of TOF

Turnover frequency is often used as a parameter for the surface activity of copper. However, the TOF, which is calculated from the methanol consumption rate and the Cu surface amount, depends on the methanol conversion because the conversion is not proportional to the contact time (W/F) (see Fig. 3) [18,19]. For example, the values for 2In-CZZ at 7 h-on-stream are 3 s^{-1} at the methanol conversion of 55% and 2 s^{-1} at 79%. In the case of 5In-CZZ, the values are 2 s^{-1} at 32% and 1 s^{-1} at 47%. Hence, the values of TOF should be compared at the same conversion.

We have experimentally found a linear fit between $1/(1 - C)$ and W/F in the range of C below 80% (Fig. 14). On the basis of the relation,

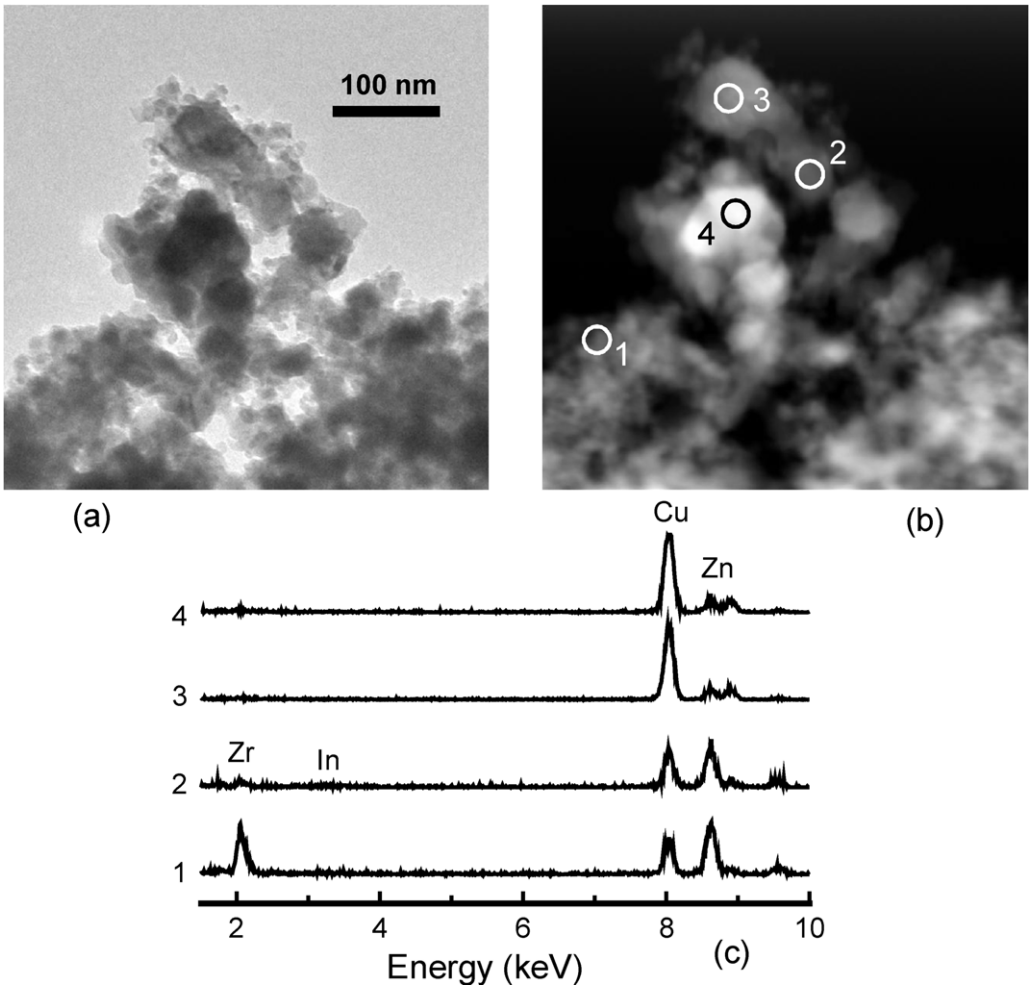

Fig. 10. TEM and HAADF/STEM images and EDS analysis of 2In-CZZ after reaction for 7 h. (a) TEM image, (b) HAADF/STEM image, and (c) EDS spectra on points 1–4.

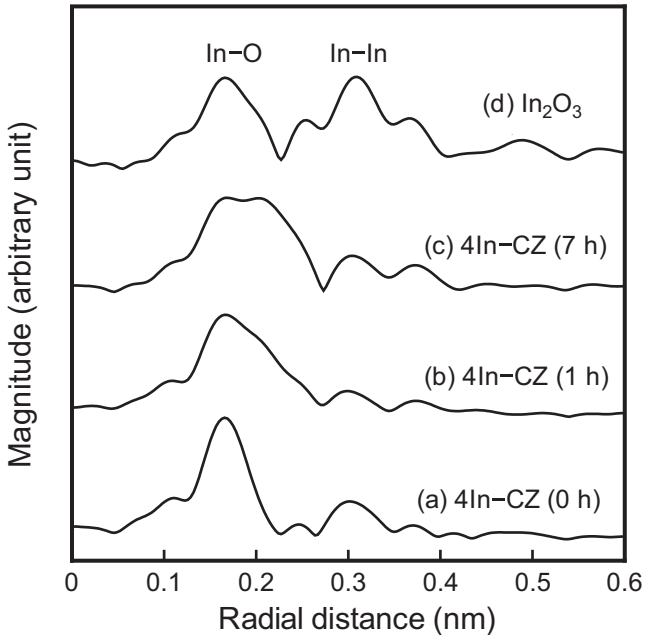

Fig. 11. Fourier transforms of k^3-weighted In K-edge EXAFS for 4In-CZ. (a) After reduction with the reaction feed at 250 °C for 1 h, (b) after reaction for 1 h, (c) after reaction for 7 h, and (d) In_2O_3 standard.

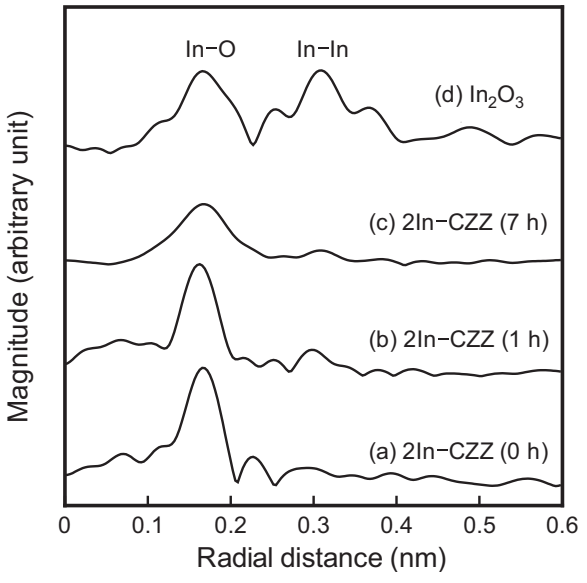

Fig. 12. Fourier transforms of k^3-weighted In K-edge EXAFS for 2In-CZZ. (a) After reduction with the reaction feed at 250 °C for 1 h, (b) after reaction for 1 h, (c) after reaction for 7 h, and (d) In_2O_3 standard.

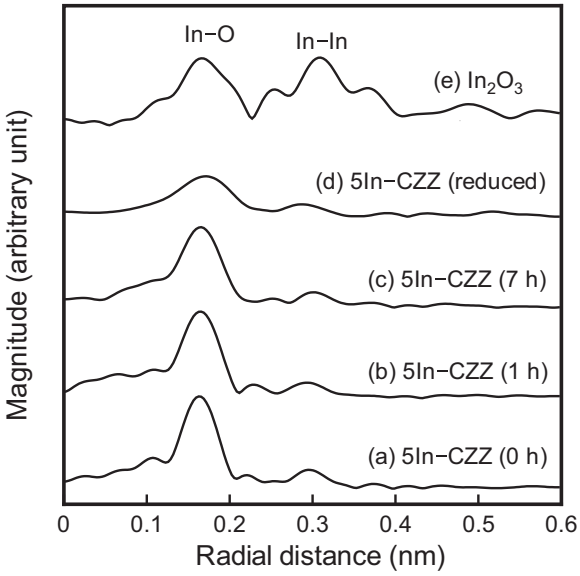

Fig. 13. Fourier transforms of k^3-weighted In K-edge EXAFS for 5In-CZZ. (a) After reduction with the reaction feed at 250 °C for 1 h, (b) after reaction for 1 h, (c) after reaction for 7 h, (d) after reduction with hydrogen at 400 °C for 1 h, and (e) In_2O_3 standard.

the value of *W*/*F* producing the methanol conversion of 50% can be estimated. Accordingly, the methanol consumption rate at the conversion of 50% is evaluated from the obtained value of *W*/*F* and the TOF is normalized at the conversion of 50% (see Table 3).

4.3. Effect of In_2O_3-addition to the activity of Cu/ZnO

No significant peaks for indium oxide are present in the XRD patterns for 4In-CZ after the reduction with the reaction feed at 250 °C (see Fig. 4b), implying presence of fine indium oxide particles. The Fourier transform of the EXAFS just after the reduction at 250 °C (see fig. 11a) is similar to that for indium oxide nanocrystals formed by ion implantation [20]. The weak In—In interaction suggests that the number of the atoms at the 2nd coordination is small, i.e., the size of the oxide is considerably small. The shape of In—O interaction is changed during the reaction and a significant shoulder is present after the reaction for 7 h (see Fig. 11c), showing formation of different species. Sintering of indium oxide is considered because a large lump containing In is observed in the TEM image of the sample after the reaction (see Fig. 9). The XRD peak at 30.6° in the pattern of 4In-CZ after the reaction is assignable to In_2O_3(1 0 4) [14], and the absence of the peak in the pattern for the sample after the reaction for 1 h (see Figs. 4c and d) evidences the sintering during the reaction. However, the sintering is partial and a significant part of In_2O_3 particles are still highly dispersed because the In—O interaction at 0.17 nm is major even after 7 h-on-stream (see Fig. 11c). Despite the structural change of indium oxide, the methanol consumption rate for 4In-CZ depends mainly on the Cu surface amount (see Table 3). The Cu surface amounts of CZ and 4In-CZ after the reaction for 7 h are calculated as 0.08 mmol g^{-1} and 0.06 mmol g^{-1}, respectively (see Table 3), suggesting that the effect of the In_2O_3 addition to the Cu surface amount is minor. On the other hand, the TOF of 4In-CZ is significantly smaller than that for CZ. Thus, the addition of indium oxide deactivates the Cu surface, and a small part of indium oxide must be in contact with the Cu surface. As shown in Fig. 8c, In is slightly detected with Cu, suggesting the presence of indium oxide nearby Cu particles. The slight detection is probably due to the low surface concentration of In^{3+} (see Table 2).

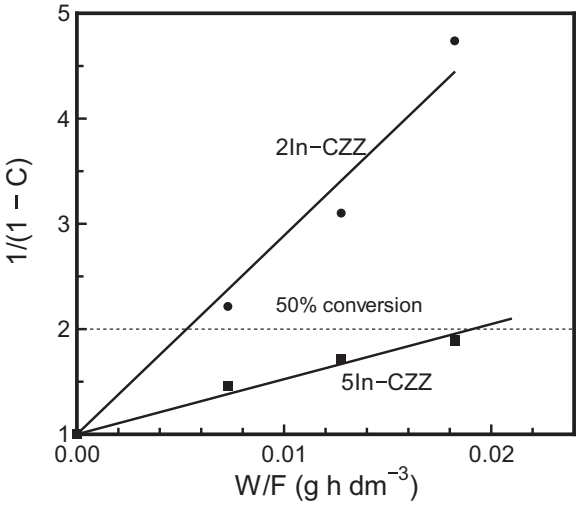

Fig. 14. Plots of $1/(1-C)$ vs. *W*/*F* for In_2O_3-modified Cu/ZnO/ZrO_2 (*C*, methanol conversion). Circle symbols, 2In-CZZ; square, 5In-CZZ.

4.4. Effect of In_2O_3-addition to the activity of Cu/ZnO/ZrO_2

It is known that the addition of zirconium oxide to Cu/ZnO causes reduction in the particle sizes of Cu and ZnO in the coprecipitated catalyst [8,9,21]. The mean crystallite sizes for Cu and ZnO of In-CZZ are significantly smaller than those for 4In-CZ and CZ (see Table 1). In addition, the higher dispersion of Cu and ZnO particles is shown in the TEM image for 2In-CZZ (see Fig. 10). No XRD peak attributed to indium oxide is present in the patterns for 2In- and 5In-CZZ after the reaction for 7 h (see Figs. 5 and 6), and there is no shoulder at 0.2 nm in the Fourier transforms of the EXAFS for In-CZZ (see Figs. 12 and 13). Hence, it is suggested that the sintering of indium oxide found in 4In-CZ does not occur in these catalysts containing zirconium oxide and the In_2O_3 particles are highly dispersed.

The BET surface areas for the In-CZZ samples are significantly higher than those for 4In-CZ (see Table 3). The Cu surface amounts are also larger, while the methanol consumption rates are unexpectedly higher than those for 4In-CZ (see Table 3). For example, the rates for 2In- and 5In-CZZ at 7 h-on-stream are 0.43 and 0.12 mmol s^{-1} g^{-1}, respectively, and that for 4In-CZ is only 0.032 mmol s^{-1} g^{-1}. The rates for In-CZZ decrease in the initial stage of the reaction at 400 °C, but they become stable after the reaction at 500 °C for 1 h. The TOF for 5In-CZZ after the stabilization is 1 s^{-1} and significantly smaller than that for 2In-CZZ (4 s^{-1}), suggesting that the presence of indium oxide causes the deactivation of Cu surface. However, the TOF for 4In-CZ is as low as 0.5 s^{-1}; hence, the presence of zirconium oxide significantly mitigates the deactivation of Cu surface with indium oxide.

The by-production of carbon monoxide is considerably suppressed in the presence of indium oxide (see Figs. 1 and 2), while addition of ZrO_2 to Cu/ZnO does not affect the selectivity significantly [8,9]. The CO formation over Cu/ZnO/Al_2O_3 is considered to be mainly due to the reverse water-gas shift (WGS) reaction, i.e., $CO_2 + H_2 \rightarrow CO + H_2O$ [18,22]. Słoczyński et al. reported that the addition of indium oxide drastically decreases the activity of Cu/ZnO/ZrO_2 to CO_2 hydrogenation [23], suggesting that the low CO selectivity in the presence of indium oxide is caused by the suppression of the reverse WGS reaction. The low CO selectivity shows that indium oxide modifies the Cu surface and changes the surface property. Kniep et al. discussed that defects such as microstrain and structural disorder in Cu particles can increase the surface activity [24]. The defects are originated from the interaction between Cu particles and ZnO, and the reduction in the surface activity of Cu/ZnO or Cu/ZnO/ZrO_2 during the reforming at 400 °C is probably

due to decrease in the interaction accompanied with the structural change such as particle sintering [8,9]. It can be hypothesized that interaction between Cu particles and indium oxide, which is highly dispersed in the catalyst, also produces the active sites with the low CO selectivity. The methane yields for 4In-CZ, 2In-, and 5In-CZZ at the end of the reaction are 0.04%, 0.02%, and 0.04%, respectively, and depend rather on the In_2O_3 contents; therefore, indium oxide may produce new sites for methane formation.

The surface oxidation state of copper often affects its activity to methanol steam reforming [25,26], but the electronic state of copper on 5In-CZZ reduced with hydrogen is almost the same as that for $Cu/ZnO/ZrO_2$ reported previously [9]. It is characteristic that the activity of 5In-CZZ reduced with hydrogen at 400 °C is low from the beginning of the reaction although the Cu surface amount is close to that for 5In-CZZ after the reaction for 1 h without the H_2 reduction (see Table 3). The TOF for 5In-CZZ just after the H_2 reduction is a half of that for the latter (see Table 3), suggesting that the H_2 reduction causes the decrease in the activity of Cu surface. As discussed in the previous section, indium oxide can be partly reduced with the H_2 reduction. The decrease in the magnitude of the In—O interaction is seen with 2In-CZZ after the reaction for 7 h, suggesting that partial reduction of indium oxide occur during the reaction at 500 °C. It is hypothesized that the partial reduction of indium oxide causes the low surface activity of copper. In the case of 5In-CZZ, the magnitude of the In—O interaction seems to decrease gradually with the increase in the time-on-stream (see Fig. 13). It is known that brass formation of Cu—Zn causes deactivation of Cu/ZnO [27]. Hence, partial formation of Cu—In alloy would reduce the activity of Cu surface although no formation of Cu—In can be evidenced in this study. The higher surface concentration of In^{3+} for 4In-CZ (see Table 2) may suggest enhancement in the partial reduction of indium oxide on the Cu surface in comparison with In-CZZ. The stoichiometric concentrations of In^{3+} for 2In- and 5In-CZZ are calculated as 0.7 and 1.7%, respectively, and significantly larger than the surface concentrations determined by XPS. On the other hand, the stoichiometric concentration for 4In-CZ is 1.4% and similar to the surface concentration. Thus, the presence of zirconium oxide may decrease the amount of the reduced In species on the surface and cause less deactivation by the addition of indium oxide. The CO selectivity is low even in the initial stage of the reaction (see Figs. 1 and 2), while the catalytic activity is high before the reaction at 500 °C. Hence, it is suggested that the nature of the active sites is not affected by the partial reduction of indium oxide and the partial reduction causes rather decrease in the number of the active sites.

5. Conclusions

Addition of indium oxide to Cu/ZnO does not affect the structure of the coprecipitated catalyst significantly, while indium oxide particles are partially aggregated during the methanol steam reforming at 400 °C or above. The Cu surface amount for Cu/ZnO modified with 4 wt.% of In_2O_3 is similar to that for the unmodified one, but the catalytic activity is greatly decreased by the In_2O_3 addition. That is, the addition of indium oxide causes the significant reduction in the TOF, although the addition stabilizes the Cu surface activity during the reaction. The addition of 5 wt.% of In_2O_3 to $Cu/ZnO/ZrO_2$ also deactivates the Cu surface. However, the catalytic activity is significantly higher than that for the In_2O_3-modified Cu/ZnO and the activity is stabilized after the reaction at 500 °C for 1 h. The TOF for the 5 wt.% In_2O_3—$Cu/ZnO/ZrO_2$ is considerably higher than that of the 4 wt.% In_2O_3—Cu/ZnO, showing that presence of zirconium oxide mitigates the deactivation of the Cu surface with indium oxide. The activity of $Cu/ZnO/ZrO_2$ containing 2 wt.% of In_2O_3 is also stable and it is as high as that for the unmodified Cu/ZnO whose activity is gradually decreased. The TOF is significantly higher than that of 5 wt.% In_2O_3—$Cu/ZnO/ZrO_2$, and the Cu surface amount is similar to that of the latter. No aggregation of indium oxide takes place during the reaction in the presence of zirconium oxide. Hence, the addition of the small amount of In_2O_3 to $Cu/ZnO/ZrO_2$ is effective to the stabilization of the Cu surface without significant reduction in the TOF. Although the addition of indium oxide results in no significant change in the electronic state of the copper surface, the presence of indium oxide suppresses by-production of carbon monoxide considerably.

References

[1] S. Hočevar, W. Summers, in: A. Léon (Ed.), Hydrogen Technology, Springer, Berlin, 2008, p. 15.
[2] N. Sirosh, A. Niedzwiecki, in: A. Léon (Ed.), Hydrogen Technology, Springer, Berlin, 2008, p. 291.
[3] C. Song, in: N. Brandon, D. Thompsett (Eds.), Fuel Cells Compendium, Elsevier, Oxford, 2005, p. 53.
[4] D.R. Palo, R.A. Dagle, J.D. Holladay, Chem. Rev. 107 (2007) 3992.
[5] Japanese Patent Kokai, 2004-292202.
[6] G. Kolios, A. Gritsch, A. Morillo, U. Tuttlies, J. Bernnat, F. Opferkuch, G. Eigenberger, Appl. Catal. B 70 (2007) 16.
[7] M. Yang, S. Li, G. Chen, Appl. Catal. B 101 (2011) 409.
[8] Y. Matsumura, H. Ishibe, Appl. Catal. B 91 (2009) 524.
[9] Y. Matsumura, H. Ishibe, J. Mol. Catal. A 345 (2011) 44.
[10] H. Lorenz, W. Jochum, B. Klötzer, M. Stöger-Pollach, S. Schwarz, K. Pfaller, S. Penner, Appl. Catal. A 347 (2010) 34.
[11] T. Umegaki, K. Kuratani, Y. Yamada, A. Ueda, N. Kuriyama, T. Kobayashi, Q. Xu, J. Power Sources 179 (2008) 566.
[12] Y. Men, G. Kolb, R. Zapf, M. O'Connell, A. Ziogas, Appl. Catal. A 380 (2010) 15.
[13] ISO 18118, 2004.
[14] JCPDS Files, 40836, 211486, 170923, and 220336.
[15] C. Hammond, The Basics of Crystallography and Diffraction, Oxford University Press, New York, 1997, p. 145.
[16] C.D. Wagner, in: D. Briggs, M.P. Seah (Eds.), Practical Surface Analysis, Auger and X-ray Photoelectron Spectroscopy, vol. 1, second ed., John Wiley & Sons, Inc., New York, 1990, p. 595.
[17] J.W. Evans, M.S. Wainright, A.J. Bridgewater, D.J. Young, Appl. Catal. 7 (1983) 75.
[18] H. Purnama, T. Ressler, R.E. Jentoft, H. Soerijanto, R. Schlögl, R. Schomäcker, Appl. Catal. A 259 (2004) 83.
[19] B.A. Peppley, J.C. Amphelett, L.M. Kearns, R.F. Mann, Appl. Catal. A 179 (1999) 21.
[20] C. Yaicle, A. Blacklocks, A.V. Chadwick, J. Perrière, A. Rougier, Appl. Surf. Sci. 254 (2007) 1343.
[21] J. Agrell, H. Birgersson, M. Boutonnet, I. Melián-Cabrera, R.M. Navarro, J.L.G. Fierro, J. Catal. 219 (2003) 389.
[22] J. Agrell, H. Birgersson, M. Boutonnet, J. Power Sources 106 (2002) 249.
[23] J. Słoczyński, R. Grabowski, P. Olszewski, A. Kozłowska, J. Stoch, M. Lachowska, J. Skrzypek, Appl. Catal. A 310 (2006) 127.
[24] B.L. Kniep, F. Girgsdies, T. Ressler, J. Catal. 236 (2005) 34.
[25] I. Ritzkopf, S. Vukojević, C. Weidenthaler, J.-D. Grunwaldt, F. Schüth, Appl. Catal A 302 (2006) 215.
[26] Y. Matsumura, H. Ishibe, Appl. Catal. B 86 (2009) 114.
[27] T. Van Herwijnen, W.A. De Jong, J. Catal. 34 (1974) 209.